NJC

ROYAL SOCIETY OF CHEMISTRY

PAPER

View Article Online
View Journal | View Issue

Cite this: *New J. Chem.*, 2023, **47**, 6844

Novel artesunate–pyrimidine-based hybrids with anticancer potential against multidrug-resistant cancer cells†

Ljiljana Koračak,[a] Ema Lupšić,[b] Nataša Terzić Jovanović,[c] Mirna Jovanović,[b] Miroslav Novakovic,*[c] Paraskev Nedialkov,[d] Antoaneta Trendafilova,[e] Mario Zlatović,[a] Milica Pešić[b] and Igor M. Opsenica*[a]

The synthesis of 17 hybrid molecules, consisting of artesunate, a derivative of naturally occurring artemisinin, and synthetic 4-aryl-2-aminopyrimidines, is described. New compounds were designed to improve the parent compounds' cytotoxic properties, activity, and selectivity. The synthesized hybrid molecules (**15a–f** with ethylenediamine linker and **16a–k** with piperazine linker), as well as their precursors – pyrimidine derivatives (**13a–f** and **14a–k**), artemisinin, and artesunate, were tested on sensitive and multidrug-resistant (MDR) human non-small cell lung carcinoma (NSCLC) cells. All hybrid compounds with piperazine linker **16a–k** were selective toward NSCLC cells and displayed IC_{50} values below 5 μM. Although they showed similar anticancer potency as artesunate, their selectivity against cancer cells was considerably improved. Importantly, **16h–k** hybrid compounds were able to evade MDR phenotype, inhibit P-glycoprotein (P-gp) activity, and increase the sensitivity of MDR NSCLC cells to doxorubicin (DOX). The inhibition of P-gp activity induced by **16h–j** was stronger than the one obtained with artesunate. Among these four hybrid compounds, **16k** was the most potent anticancer agent with similar IC_{50} values of around 1.5 μM (for comparison – over 3.1 μM for artesunate) in sensitive and MDR NSCLC cells.

Received 28th January 2023,
Accepted 15th March 2023

DOI: 10.1039/d3nj00427a

rsc.li/njc

Introduction

Natural products possess complex molecular architecture and high functional density, which are necessary for their strong and selective interactions with biomolecular targets. Since at least the late 1990s, it was clear that compounds resembling natural products or those exploiting natural product motifs or topologies were invaluable in medicinal chemistry.[1] Due to increasing resistance to currently available drugs, developing new effective medications with improved pharmacological properties is crucial.[2] Almost 50% of anticancer drugs launched between the 1940s and 2014 were inspired by, or based on, natural products.[3] Even though natural products are good lead-compounds, additional chemical synthetic transformations are needed to obtain "tailor-made" final structures.[4] To this end, it has often been proven useful to fuse two different pharmacophores, where one or both may be inspired by naturally occurring molecules. The concept of hybrid molecules has moved on from its initial concept (one component targets a specific location within the patient, while the other exercises biological activity), and now enables significant improvements in the physicochemical and pharmacokinetic properties of the compound, such as ADMET, solubility, acidity, or biding constants to the target.[5] In 1972, artemisinin **1**, a natural sesquiterpene lactone, was isolated for the first time from *Artemisia annua* (sweet wormwood), a plant used in traditional Chinese medical practice to treat fever (Fig. 1).[6] Artemisinin was discovered by Prof. Youyou Tu in a project focused on developing antimalarial medications. For her work, Prof. Tu received the Nobel Prize in Physiology or Medicine in 2015.[7] Derivatization of artemisinin at the C-10 position has led to the synthesis of several new compounds including dihydroartemisinin **2**, artemether **3**, arteether **4**, and artesunic acid (artesunate) **5** (Fig. 1).[8]

[a] *Faculty of Chemistry, University of Belgrade, PO Box 51, Studentski trg 16, 11158 Belgrade, Republic of Serbia. E-mail: igorop@chem.bg.ac.rs*
[b] *Institute for Biological Research "Siniša Stanković" – National Institute of Republic Serbia, University of Belgrade, Despota Stefana 142, 11060 Belgrade, Republic of Serbia*
[c] *Institute of Chemistry, Technology and Metallurgy, National Institute of the Republic of Serbia, University of Belgrade, Njegoševa 12, 11000 Belgrade, Republic of Serbia. E-mail: mironov@chem.bg.ac.rs*
[d] *Department of Pharmacognosy, Faculty of Pharmacy, Medical University of Sofia, 2, Dunav St., 1000 Sofia, Bulgaria*
[e] *Institute of Organic Chemistry with Centre of Phytochemistry, Bulgarian Academy of Sciences, Acad. G. Bonchev St, Bl. 9, 1113, Sofia, Bulgaria*

† Electronic supplementary information (ESI) available. See DOI: https://doi.org/10.1039/d3nj00427a

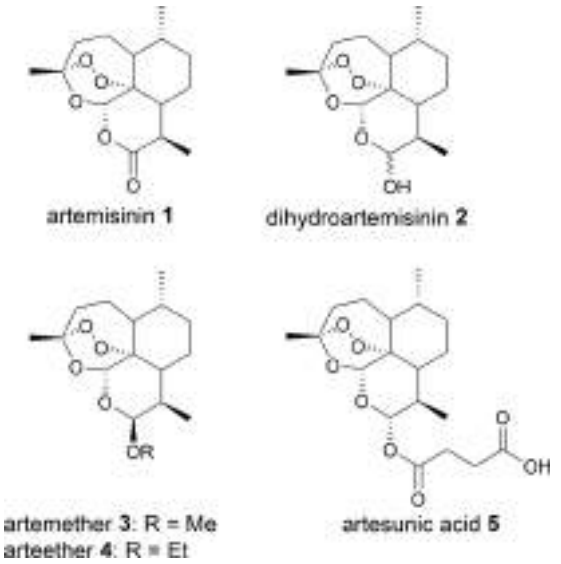

Fig. 1 Structures of artemisinin **1** and its derivatives.

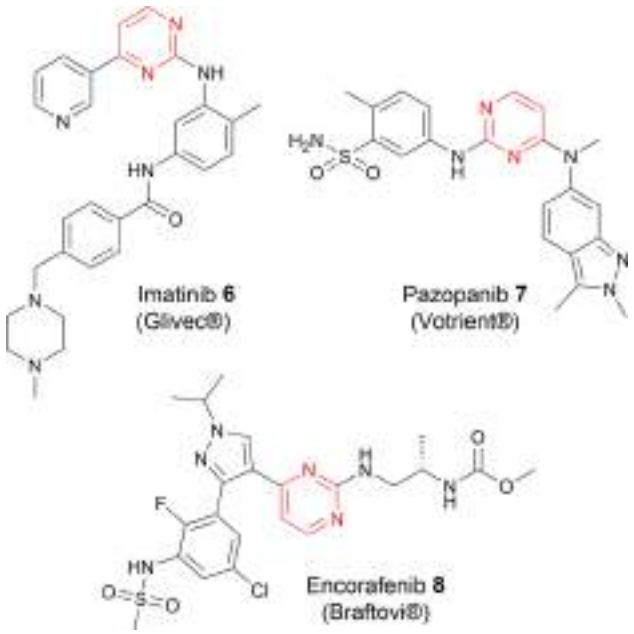

Fig. 2 Pyrimidine-containing drugs in cancer therapy.

The synthesis of new artemisinin derivatives is of significant interest in medicinal chemistry due to the low bioavailability and unfavorable pharmacokinetic profile of artemisinin.[9] Artesunate **5**, a semisynthetic compound is obtainable from artemisinin **1** *via* the reduction of artemisinin into dihydroartemisinin **2** followed by esterification using succinic anhydride.[10] Compared to artemisinin, artesunate displayed improved absorption, solubility, and pharmacokinetics.[11] Investigations of the biological activity of artemisinin and artesunate derivatives have shown that, in addition to being used for the effective treatment of malaria, these derivatives exhibited also anticancer activity against a wide variety of cancer cell lines, such as leukemia, melanoma, lung, colon, renal, ovarian, prostate, and breast, as well as the potential for the treatment of lupus and activity against several viruses.[12] The endoperoxide bridge is the key structural moiety of artemisinin derivatives responsible for their antimalarial and anticancer activity.[13] The mechanisms *via* which artesunate induces anticancer activity and its impact on cell death include: autophagy and apoptosis induction, antiangiogenesis, ferroptosis, and proliferation inhibition.[11,13]

The pyrimidine scaffold is an important building block in medicinal chemistry, being present in numerous biologically active compounds with anticancer, antiviral, antibacterial, anti-inflammatory, and antimalarial activity. The importance of substituted pyrimidines is evidenced by the presence of the pyrimidine moiety in many natural products and approved drugs.[14,15] Additionally, pyrimidine derivatives show promising anticancer activity as reflected in the number of pyrimidine-containing FDA-approved drugs (Fig. 2) such as Imatinib (Glivec®) **6**, Pazopanib (Votrient®) **7**, Encorafenib (Braftovi®) **8**, as well as many drug candidates undergoing clinical phase trials.[16]

Globally, lung cancer is the deadliest cancer with 18.4% of all cancer-related deaths according to World Health Organization 2020.[17] The diagnosis is usually made in the advanced stage of the disease and therefore the 5 year survival rate is low (10–20% for the majority of countries in the world).[18] Additionally, lung cancer is hard to treat due to the development of multidrug resistance (MDR).[19] The most relevant mechanism of MDR is the overexpression and increased activity of P-glycoprotein (P-gp) which acts as a membrane transporter capable to extrude various xenobiotics as well as anticancer agents.[20] P-gp contributes to the acquired MDR developed after chemotherapy and targeted therapy in many different cancer types including non-small cell lung carcinoma (NSCLC).[21] Although advances in sequencing technology and target identification enabled the implementation of personalized therapy approaches, only 3–9% of NSCLC patients respond to recommended targeted therapy.[22] Therefore, other approaches for the achievement of optimal therapy should be considered. Artesunate and some of its newly reported derivatives showed considerable activity against P-gp in cancer cells.[23,24] Therefore, our aim was to elucidate whether hybrid compounds formed of two well-known anticancer pharmacophores (artesunate and pyrimidine) interact with the MDR phenotype in NSCLC cells and modulate the P-gp activity. Preferable anticancer features of novel compounds should include low or no resistance in MDR cancer cells, inhibitory or evading activity against P-gp, and high selectivity toward cancer cells. To that end, a pair of sensitive (NCI-H460 without P-gp expression) and MDR (NCI-H460/R with P-gp expression) NSCLC cell lines, and lung fibroblast cells (MRC-5), as control normal cells, comprised a model system for our investigations.

Results and discussion

Chemistry

Our study aimed to develop an efficient method for synthesizing new artesunate derivatives with improved pharmacological

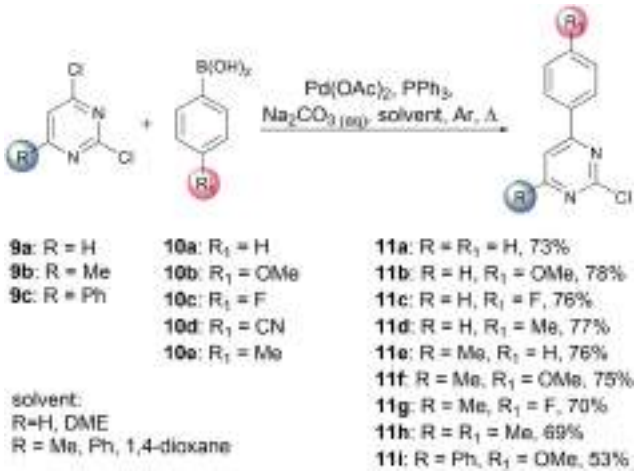

Scheme 1 Suzuki–Miyaura cross-coupling reaction of 2,4-dichloropyrimidines **9a–c** with arylboronic acids **10a–e**.

properties by connecting two pharmacophores (artesunic acid and pyrimidine derivatives).

In order to obtain pyrimidine derivatives, which would later be connected with artesunic acid, commercially available 2,4-dichloropyrimidines **9a–c** were coupled with different arylboronic acids **10a–e** in the presence of the palladium catalyst. Products of the Suzuki–Miyaura reaction **11a–i** were obtained in good yields (Scheme 1).[25] With the aim to further derivatize the pyrimidine core and create a linkage point for the artesunic acid, diamino moiety was introduced in the C-2 position. Compounds **11a–i** were subjected to nucleophilic aromatic substitution with different mono Boc-protected amines **12a** and **12b**[26] in the presence of K_2CO_3 and 1,4-dioxane (Scheme 2). The desired pyrimidine derivatives **13a–f** and **14a–k** were obtained in good to excellent yields upon *N*-deprotection of an amino group using TFA (Scheme 2). We envisioned that the connection between artesunic acid and pyrimidine derivatives would be accomplished *via* amide bond formation, which will result in the synthesis of hybrid molecules that contain two pharmacophores (artesunic acid and pyrimidine scaffold, Scheme 3). The amide bond formation is commonly applied in the synthesis of hybrids owing to its simplicity, stability, high product yield and selectivity. Using this methodological approach, artesunic acid **5** was reacted with different pyrimidine derivatives, **13a–f** with ethylenediamine linker, as well as **14a–k** with piperazine linker, in the presence of HOBt and EDCI at room temperature and the target compounds **15a–f** and **16a–k** were synthesized in moderate to good yields.[27]

Biological evaluation

Preliminary screening of artemisinin, artesunate, pyrimidine derivatives and corresponding hybrid compounds. Preliminary screening of **13a–f**, **14a–k**, **15a–f**, and **16a–k** was performed on sensitive NCI-H460 and resistant NCI-H460/R cells using two concentrations of 5 μM and 30 μM (Fig. 3 and Fig. S1 ESI,† respectively). The cell growth inhibition levels achieved by novel compounds were compared with levels obtained by artemisinin and artesunate (Fig. 3 and Fig. S1, ESI†).

Preliminary screening showed that hybrid compounds (**15a–f** and **16a–k**) were more potent anticancer agents than pyrimidine derivatives (**13a–f** and **14a–k**) (Fig. 3 and Fig. S1, ESI†). Upon 5 μM treatment, almost all hybrid compounds (with an exception of **15a**) reached 50% of cell growth inhibition in NCI-H460. Among pyrimidine derivatives, only **14k** inhibited the growth of NCI-H460 cells by more than 50%. Worth noting, **14k** was the most potent anticancer agent (it reached around 90% of cell growth inhibition) showing no

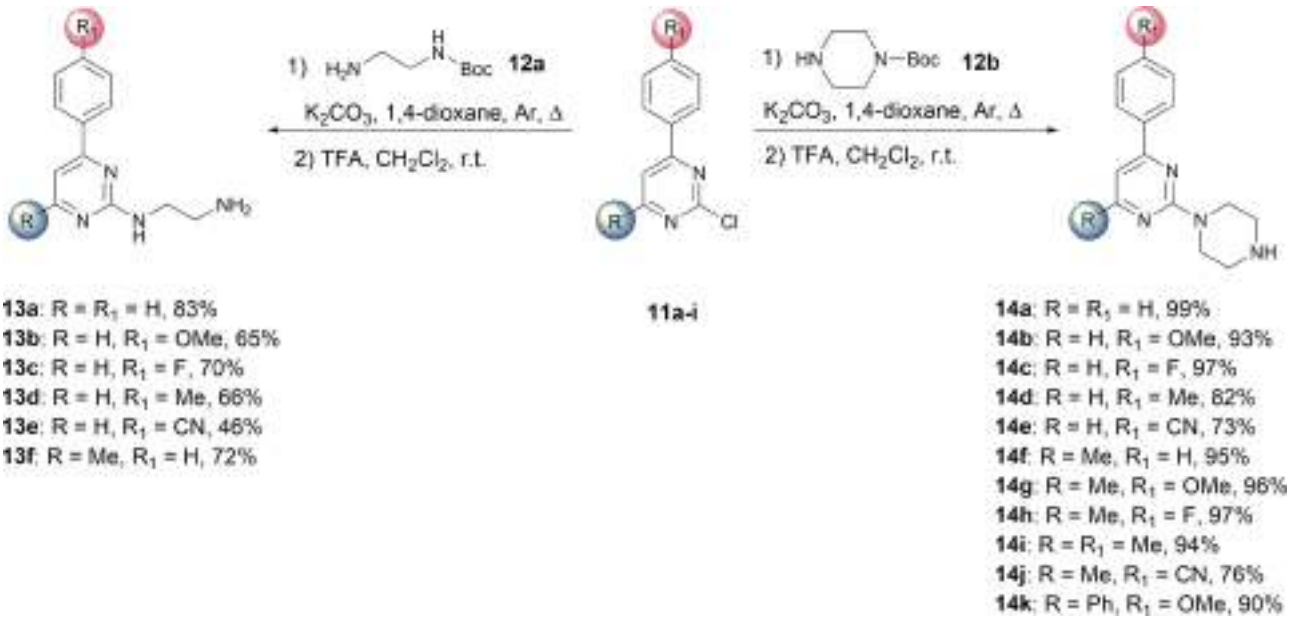

Scheme 2 Synthesis of 4-aryl-2-aminopyrimidines **13a–f** and **14a–k**.

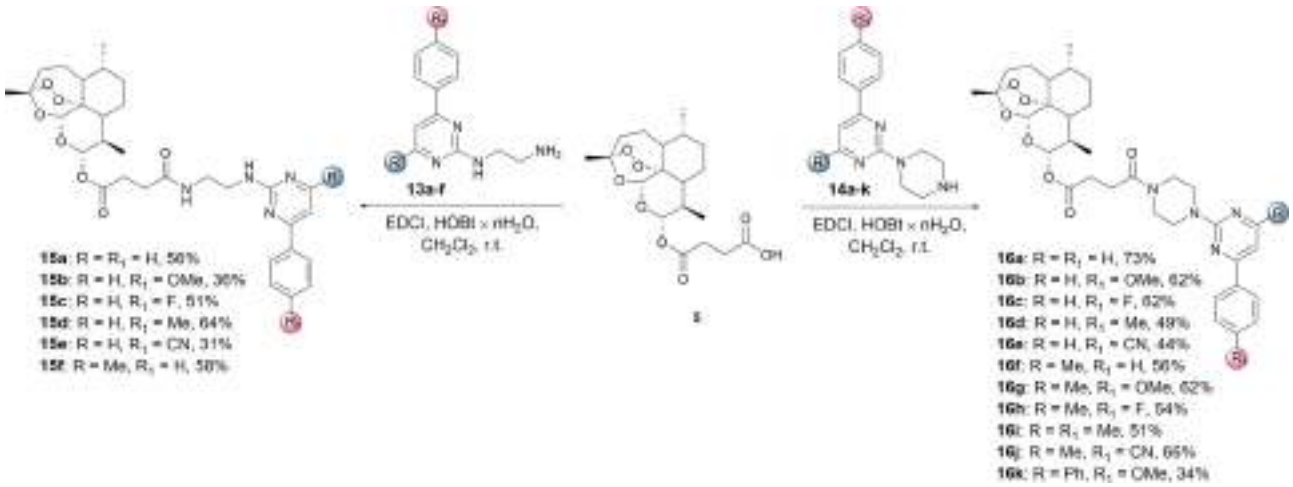

Scheme 3 Synthesis of new artesunate-based hybrids **15a–f** and **16a–k**.

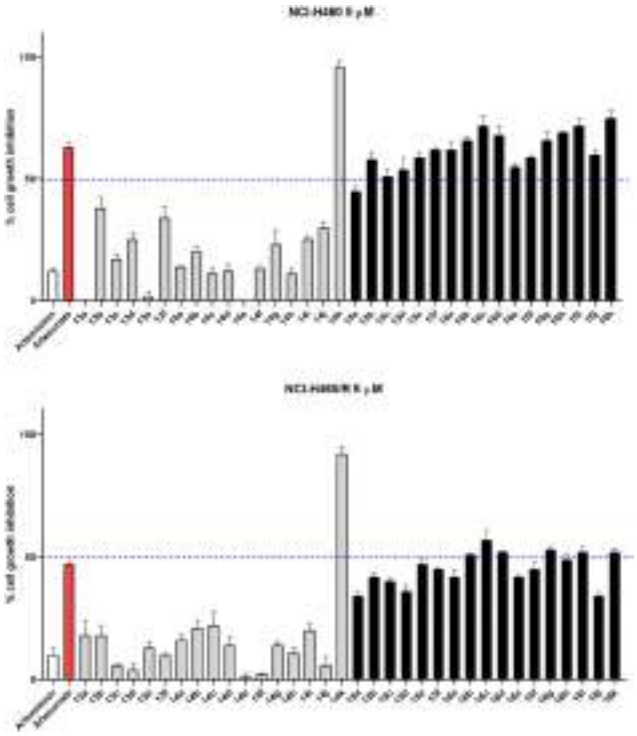

Fig. 3 Preliminary screening of novel pyrimidine derivatives and hybrid compounds. Artemisinin (white bar), artesunate (red bar), **13a–f** and **14a–k** (grey bars), and **15a–f** and **16a–k** (black bars) were applied to NCI-H460 and NCI-H460/R cells at a concentration of 5 μM. The average percentage of cell growth inhibition and standard deviation were calculated according to MTT results assayed after 72 h treatment ($n \geq 3$). The blue dashed line indicates 50% of cell growth inhibition.

difference in the sensitivity of NCI-H460 and NCI-H460/R cells. Since **14k** was the only 6-phenyl pyrimidine derivative among 11 derivatives of this type, the possible activity could be ascribed to this phenyl substituent. Artemisinin had a poor effect on both cell lines, while artesunate achieved a considerable level of the cell growth inhibition (above 50% in NCI-H460 cells). The sensitivity of NCI-H460 and NCI-H460/R cells to novel compounds differed. The majority of compounds showed decreased efficacy in resistant NCI-H460/R cells (Fig. 3).

Assessment of resistance profile and selectivity toward cancer cells. Pyrimidine derivative **14k** and all hybrid compounds (**15a–f** and **16a–k**) were selected for the examination of resistance and selectivity profiles according to "Relative Resistance" and "Selectivity Index", respectively (Table 1). Cell growth inhibition of sensitive NCI-H460, resistant NCI-H460/R, and normal MRC-5 cells induced by the concentration range of artemisinin, artesunate, and selected compounds was assessed by MTT and evaluated by IC_{50} values (Table 1 and Fig. S2, S3, ESI†).

Artesunate showed a significant anticancer potential with IC_{50} values lower than 5 μM in both cancer cell lines. The effect of artemisinin was poor with IC_{50} values over 100 μM. Both artesunate and artemisinin effects were not compromised in NCI-H460/R cells whose resistance was induced by doxorubicin (DOX) application.[28] However, other authors showed a significant resistance to artesunate in doxorubicin-resistant leukemia cells (K562/ADR).[23] Additionally, artemisinin and artesunate were not selective against NSCLC cells. A recent publication reported similar results with artesunate showing no selectivity against breast cancer cells (MCF-7) in comparison with MRC-5 cells.[29] Pyrimidine derivative **14k** and hybrid compounds **16a–k** exhibited $IC_{50} < 5$ μM in sensitive NCI-H460 cells, while for hybrid compounds **15a–f** IC_{50} values ranged 5–10 μM. The presence of the MDR phenotype significantly affected the efficacy of eight hybrid compounds (**15a** and **16a–g**) with "Relative Resistance" higher than 2. Importantly, all hybrid compounds with piperazine linker (**16a–k**) showed good selectivity profiles, suggesting piperazine substructure as an important part of pharmacophore. Although the selectivity of **16a–k** was less than that obtained by DOX, NCI-H460/R cells were less resistant to hybrid compounds in comparison with DOX (Table 1).

Interaction with P-glycoprotein activity. The interaction of artemisinin, artesunate, **14k**, **15a–f**, and **16a–k** with P-gp activity was studied in resistant NCI-H460/R cells by rhodamine 123

Table 1 Resistant and selectivity profiles of artemisinin, artesunate, **14k**, **15a–15f**, and **16a–16k** according to IC_{50} values obtained in NCI-H460, NCI-H460/R, and MRC-5 cells

	NCI-H460	NCI-460/R[a]	Relative resistance	MRC-5[b]	Selectivity index
Artemisinin[c]	202.0 ± 4.710	215.7 ± 2.605	1.07	322.1 ± 5.934	1.59
Artesunate[d]	3.134 ± 0.034	4.131 ± 0.049	1.32	5.757 ± 0.088	1.84
14k	2.019 ± 0.050	3.811 ± 0.077	1.90	3.471 ± 0.086	1.72
15a	5.571 ± 0.069	16.423 ± 0.229	2.95[f]	10.295 ± 0.138	1.85
15b	5.467 ± 0.074	6.063 ± 0.075	1.09	8.426 ± 0.154	1.54
15c	7.120 ± 0.086	13.337 ± 0.130	1.87	10.360 ± 0.159	1.45
15d	7.002 ± 0.109	7.745 ± 0.942	1.11	11.182 ± 0.110	1.60
15e	5.853 ± 0.073	10.030 ± 0.102	1.71	7.701 ± 0.133	1.32
15f	6.319 ± 0.109	8.477 ± 0.124	1.34	9.743 ± 0.086	1.54
16a	3.059 ± 0.045	13.936 ± 0.193	4.55[f]	11.256 ± 0.117	3.68[g]
16b	2.476 ± 0.045	11.768 ± 0.153	4.75[f]	12.248 ± 0.220	4.95[g]
16c	1.234 ± 0.019	2.892 ± 0.042	2.34[f]	9.160 ± 0.157	7.42[g]
16d	2.040 ± 0.048	12.501 ± 0.206	6.13[f]	12.582 ± 0.336	6.17[g]
16e	3.071 ± 0.43	8.185 ± 0.087	2.66[f]	13.130 ± 0.137	4.27[g]
16f	1.759 ± 0.042	5.422 ± 0.076	3.09[f]	8.993 ± 0.156	5.11[g]
16g	1.870 ± 0.035	8.361 ± 0.197	4.47[f]	8.392 ± 0.178	4.48[g]
16h	2.321 ± 0.046	4.312 ± 0.081	1.85	6.859 ± 0.159	2.95[g]
16i	2.219 ± 0.053	4.323 ± 0.101	1.95	7.299 ± 0.195	3.29[g]
16j	3.582 ± 0.057	6.084 ± 0.108	1.70	9.212 ± 0.118	2.57[g]
16k	1.507 ± 0.058	1.661 ± 0.061	1.10	5.517 ± 0.209	3.66[g]
DOX[e]	61.13 ± 0.52	524.54 ± 8.91	8.58[f]	588.00 ± 15.85	9.62[g]

[a] NCI-H460/R cells with high P-gp expression were selected from NCI-H460 cells with null P-gp expression by their continuous culturing in a medium containing stepwise increasing concentrations of DOX for three months. [b] Normal cells: human lung fibroblasts (MRC-5). [c] Concentration range for artemisinin: 5, 10, 25, 50, and 100 μM. [d] Concentration range for artesunate and all artesunate derivatives: 1, 2.5, 5, 10, and 25 μM. [e] Concentration range for DOX: 100, 250, 500, 1000, and 2000 nM. [f] Resistance: the IC_{50} value for the indicated compound is at least two-fold higher in the resistant cells compared to the IC_{50} value obtained in corresponding sensitive cells. [g] Selectivity toward cancer cells: the IC_{50} value for the indicated compound is at least two-fold higher in normal (non-cancer) MRC-5 cells than the IC_{50} value obtained in sensitive NCI-H460 cancer cells.

accumulation assay (Table 2, Fig. 4, and Table S1, Fig. S4, ESI†). High P-gp expression and activity are main characteristics of the NCI-H460/R cells' MDR phenotype.[28,30]

Artesunate applied at 5 μM increased rhodamine 123 accumulation 2-folds in NCI-H460/R cells. A comparable result with 10 μM artesunate was achieved in K562/ADR cells.[23] Beside artesunate, among pyrimidine derivatives, only **14b**, **14f**, and **14k** significantly increased rhodamine 123 accumulation. In contrast, the majority of hybrid compounds were able to increase rhodamine 123 accumulation (**15c**, **15d**, **16a–d**, and **16f–k**). Importantly, **14k**, **15d**, **16b–d**, and **16f–j** were more potent in inhibiting P-gp function than artesunate. Results obtained by MTT assay (IC_{50} values) and rhodamine 123 accumulation (interaction with P-gp activity) revealed four types of compounds: (i) capable to evade MDR and inhibit the P-gp activity (artesunate, **14k**, **15c**, **15d**, and **16h–k**); (ii) capable to evade MDR but without effect on P-gp activity (**15b**, **15e**, and **15f**); (iii) affected by MDR as P-gp substrates that can act as P-gp competitive inhibitors (**16a–d**, **16f**, and **16g**); (iv) affected by MDR as P-gp substrates showing no interaction with P-gp activity (**15a** and **16e**) (Table 2, Fig. 4 and Table S1, ESI†).

Other artesunate hybrid compounds were also shown either not to interact with MDR phenotype or to inhibit P-gp activity.[31]

According to MTT and rhodamine 123 accumulation results, we chose two representative compounds **16d** (a possible P-gp substrate) and **16k** (a possible P-gp inhibitor) to compare their concentration-dependent effects on P-gp activity with artesunate (as a parental compound) and TQ (as a well-known P-gp inhibitor) (Fig. 5). The artesunate effect was weak in comparison to **16d**, **16k**, and TQ (Fig. 5A and B). It did not show a concentration-dependent effect. On contrary, the effects of **16d**, **16k**, and TQ were concentration-dependent. Worth noting, **16d** was more efficient in increasing rhodamine 123 than TQ (Fig. 5A and B). Hybrid compound **16k** identified as a possible P-gp inhibitor capable to evade MDR showed a similar profile of rhodamine 123 accumulation as TQ (Fig. 5B).

To confirm that the effect of hybrid compounds **16a–g** is affected by P-gp activity, a possible reversal of resistance by 50 nM of tariquidar (TQ) was studied in NCI-H460/R cells (Fig. S5, ESI†). The reversal of resistance was observed for all tested hybrids except **16e**, the only compound with no effect on the P-gp function (Table 2 and Table S1, ESI†). The sensitivity of other compounds **16a–d**, **16f**, and **16g**, which we assumed to be P-gp substrates, increased in concurrent treatment with TQ in NCI-H460/R cells. The best resistance reversal by TQ was obtained for **16a** (Fig. 6A), while **16c** and **16f** were the least prone to increase the sensitivity. Importantly, the ''Relative Resistance'' factors of **16c**, **16e**, and **16f** were lesser than that obtained for **16a**, **16b**, **16d**, and **16g** (Table 1), and this can explain the differences in TQ-mediated restoration of sensitivity. However, 50 nM of TQ did not achieve the maximal effect and did not completely restore the sensitivity of hybrid compounds to the level obtained in sensitive NCI-H460 cells (Fig. S5, ESI†) implying that other mechanisms besides P-gp activity are involved in the resistance of NCI-H460/R cells to **16a–g**.

To confirm that **16h–k** can influence (decrease) the P-gp activity, these hybrid compounds were combined with DOX, a

Table 2 Interaction with P-gp activity assessed by rhodamine 123 accumulation assay (30 min simultaneous treatment with tested compounds)

Cell lines/compounds	MFI[a]	FAR ± S.E.[b]
NCI-H460[c]	340 061	11.57 ± 0.46
NCI-H460/R	29 394	—
Artemisinin	52 361	1.78 ± 0.15
Artesunate^{INH}	63 674	2.17 ± 0.16
TQ[d]	390 460	13.28 ± 0.58
14k^{INH}	128 209	4.36 ± 0.21
15a	54 489	1.85 ± 0.16
15b	46 478	1.58 ± 0.19
15c^{INH}	67 715	2.30 ± 0.21
15d^{INH}	91 112	3.10 ± 0.20
15e	33 825	1.15 ± 0.13
15f	39 075	1.33 ± 0.12
16a^{SUB}	76 266	2.59 ± 0.19
16b^{SUB}	143 802	4.89 ± 0.28
16c^{SUB}	114 129	3.88 ± 0.24
16d^{SUB}	99 563	3.39 ± 0.20
16e	33 757	1.15 ± 0.12
16f^{SUB}	111 450	3.79 ± 0.22
16g^{SUB}	132 961	4.52 ± 0.30
16h^{INH}	109 620	3.73 ± 0.28
16i^{INH}	147 315	5.01 ± 0.36
16j^{INH}	147 583	5.02 ± 0.31
16k^{INH}	83 011	2.82 ± 0.19

[a] The measured mean fluorescence intensity (MFI) was used to calculate the fluorescence activity ratio (FAR). [b] *Via* the following equation: FAR = MFI of MDR treated/MFI of MDR control. [c] Sensitive cancer cell line and its MDR counterpart used in the study: non-small cell lung carcinoma-NSCLC (NCI-H460 and NCI-H460/R). [d] TQ (tariquidar) as a third generation P-gp inhibitor was applied as a positive control for P-gp inhibition. ^{INH}Compounds that evade the MDR phenotype and inhibit P-gp activity (according to MTT assay and rhodamine 123 assay results). ^{SUB}Compounds whose IC_{50} value is significantly higher in MDR than in sensitive cells (showing resistant profile according to MTT assay) but at the same time capable to increase rhodamine 123 accumulation.

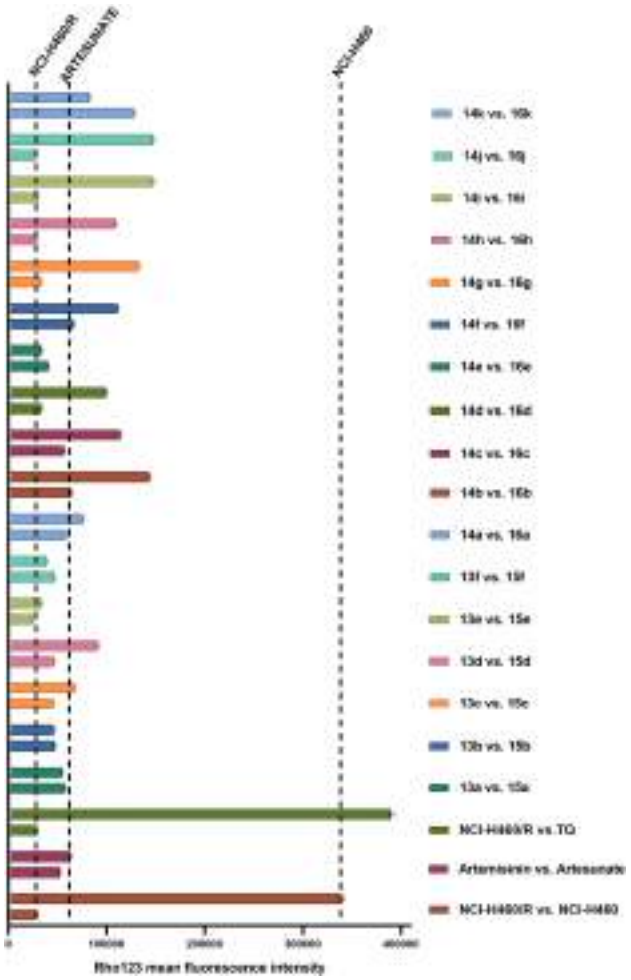

Fig. 4 Interaction with P-gp activity compared between pyrimidine derivatives and corresponding hybrid compounds. The mean fluorescence intensity (MFI) of rhodamine 123 was assessed 30 min after incubation of rhodamine 123 (2 μM) with tested compounds (5 μM). Sensitive NCI-H460 cells and resistant NCI-H460/R cells treated with 50 nM TQ served as a positive control for rhodamine 123 accumulation. Dashed lines indicate the levels of rhodamine 123 accumulation in untreated resistant NCI-H460/R cells, NCI-H460/R cells treated with artesunate, and in untreated NCI-H460 cells. Corresponding artesunate derivatives and hybrid compounds are presented with the same color. Rhodamine 123 accumulation was assessed by flow cytometry on the green channel (emission at 525 nm) and at least 10 000 events (cells) were assayed per sample.

P-gp substrate. All compounds showed a significant potential to reverse DOX resistance in NCI-H460/R cells (Fig. 6B) when applied in a concentration of 500 nM, a concentration significantly below their IC_{50} values (Table 1). The best effect was achieved with **16i** and **16j** with the highest FAR values (Table 2 and Table S1). Actually, the efficacy of **16h–k** to reverse DOX resistance (Fig. 6B) was proportional to their FAR values (Table 2 and Table S1, ESI†).

Structure–activity relationship (SAR) of synthesized compounds. Based on the results presented in Tables 1, 2 and Table S1 (ESI†) some general structure-activity relationship (SAR) patterns were found: (i) by comparing hybrid molecules **16a–k** with artesunate, it could be concluded that the introduction of the pyrimidine core with piperazine linker led to a substantial improvement in activity toward the NCI-H460 cell line in almost all hybrid compounds. On the other hand, only two hybrid molecules **16c** and **16k** were more potent than artesunate toward the NCI-H460/R cell line. Artesunate has a more favorable resistance profile in comparison to hybrids **16a–j**, with exception of **16k**. Notably, all hybrid molecules with piperazine linker (**16a–k**) have a better selectivity index than artesunate; (ii) all hybrid molecules **15a–f** and **16a–k** showed improved activity in comparison to their corresponding pyrimidine parent derivatives **13a–f** and **14a–k;** (iii) by comparing hybrids with the same substituent on the pyrimidine core (**15a–f** *vs.* **16a–f**), it could be concluded that the hybrid molecules with the piperazine linker were more potent than hybrid molecules with the ethylenediamine linker toward the NCI-H460 cell line. These results emphasize the importance of linker in hybrid molecules for biological activity; (iv) the electronic effects of the substituents (–OMe, –Me, –F, –CN) on the phenyl group attached to the pyrimidine core do not appear to significantly affect the activity; (v) the most active hybrid compound **16k** and most active pyrimidine parent compound **14k** possess phenyl group at the C6 position of pyrimidine scaffold; (vi) all hybrid molecules with the piperazine linker **16a–k** were significantly more selective toward

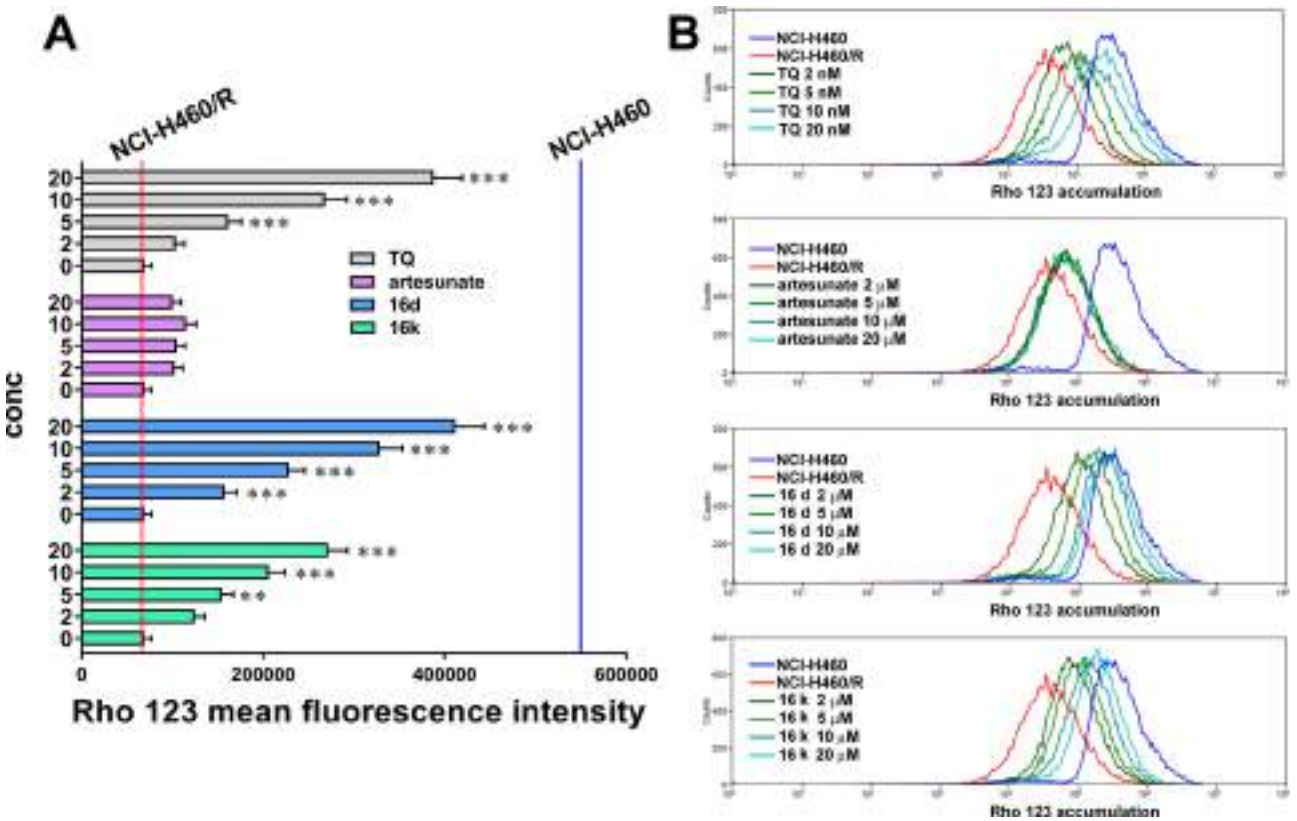

Fig. 5 Concentration-dependent effect on P-gp activity compared among tariquidar, artesunate, and two selected hybrid compounds. (A) The mean fluorescence intensity (MFI) of rhodamine 123 was assessed 30 min after incubation of rhodamine 123 (2 μM) with four increasing concentrations of tested compounds (2, 5, 10, and 20 μM for artesunate, **16d**, and **16k**; 2, 5, 10, and 20 nM for TQ). Sensitive NCI-H460 cells served as a positive control for rhodamine 123 accumulation. The red line indicates the level of rhodamine 123 accumulation in untreated resistant NCI-H460/R cells, while the blue line indicates the level of rhodamine 123 accumulation in untreated NCI-H460 cells. (B) Corresponding flow cytometry profiles illustrate the concentration-dependent effects of tested compounds. Rhodamine 123 accumulation was assessed by flow cytometry on the green channel (emission at 525 nm) and at least 20 000 events (cells) were assayed per sample. A statistically significant difference between treatments and untreated control (NCI-H460/R) was assessed by two-Way ANOVA Bonferroni multiple comparison test: $p < 0.01$ **, $p < 0.001$ ***.

NSCLC cells than the hybrids with the ethylenediamine linker **15a–f** and parent compound artesunate; (vii) hybrids **16c** and **16k** are the most active compounds. Hybrid **16k** has a favorable resistance profile, while hybrid **16c** is the most selective among hybrid molecule; (viii) according to FAR values (Table 2 and Table S1, ESI†), almost all hybrid molecules with the piperazine linker **16a–f** modulated P-gp activity more prominently than their corresponding hybrids with the ethylenediamine linker **15a–f**; (ix) presence of methyl group at the C6 position of pyrimidine scaffold contributed to increased activity of **16f–j** against P-gp in comparison with the corresponding hybrids not substituted at the C6 position **16a–e** as well as **16k** with phenyl group at the C6 position.

***In silico* studies.** Physicochemical descriptors for synthesized compounds, generated using the SwissADME website, showed that none of the hybrids break more than one Lipinski's RO5 (Table S2, ESI†). Furthermore, considering that the calculated topological polar surface area (TPSA) and log *P* values are in range of 112.55–121.78 Å^2 and 3.56–4.43 for compounds **16a–d** and **16f–i**, it can be concluded that these hybrids have a high probability of being passively absorbed by the gastrointestinal tract (Fig. S6, ESI†).[32] The rest of the compounds are predicted not to be absorbed by the gastrointestinal tract. None of the synthesized hybrids are predicted to be blood–brain barrier penetrant or to evade P-gp activity, while artemisinin and artesunate showed these preferable characteristics. However, our study identified compounds capable to evade MDR and inhibit the P-gp activity (artesunate, **14k**, **15c**, **15d**, and **16h–k**) implying that results obtained in biological systems do not resemble results obtained by SwissADME. Considering that our cancer model includes a pair of NSCLC cell lines (sensitive and MDR) with differences in P-gp expression and activity, our experimental results offer more confident results than that obtained by SwissADME. Even more, artesunate identified in our study as a possible P-gp inhibitor did not show a concentration-dependent effect on P-gp activity contrary to **16d**, **16k**, and TQ, while its effect was significantly weaker than that obtained for **16d**, **16k**, and TQ (Fig. 5). Without our experimental work, SwissADME would lead to the wrong conclusion that artemisinin and artesunate have better properties against P-gp than our compounds. We performed docking simulations of representative hybrid

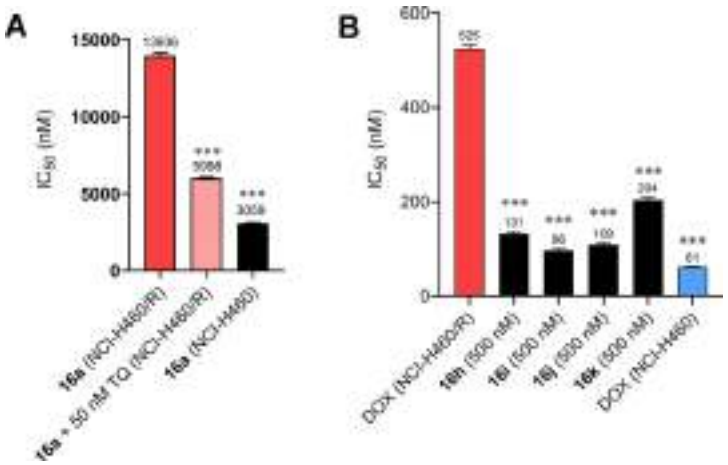

Fig. 6 (A) Reversal of a hybrid compound **16a** resistance by TQ. The effect of **16a** in NCI-H460/R cells (red bar), in NCI-H460 cells (black bar), and in concurrent treatment with 50 nM TQ in NCI-H460/R cells (light red bar). Hybrid compound **16a** was tested in the concentration range 1–25 μM, assayed by MTT after 72 h treatment ($n \geq 3$), and analyzed by non-linear regression in GraphPad Prism 8. Statistical significant difference compared to **16a** concentration-dependent effect in NCI-H460/R was calculated by Dunnett's multiple comparisons test: *** ($p < 0.001$). (B) Reversal of DOX resistance by hybrid compounds **16h–k**. DOX (100–2000 nM) in combination with 500 nM **16h–k** was assayed by MTT after 72 h treatment ($n \geq 3$) and analyzed by non-linear regression in GraphPad Prism 8. The blue bar represents the IC_{50} value for DOX obtained in sensitive NCI-H460 cells, the red bar in MDR NCI-H460/R cells, and the black bars represent IC_{50} values for DOX obtained in combination with **16h–k** in NCI-H460/R cells. Statistical significant difference compared to DOX concentration-dependent effect in NCI-H460/R was calculated by Dunnett's multiple comparisons test: *** ($p < 0.001$).

compounds **16d** (identified as a possible P-gp substrate) and **16k** (identified as a possible P-gp inhibitor). Both **16d** and **16k** bind in same space but, due to differences in size and functionalities, they interact with different amino acid residues (Fig. 7A and C). In both cases, most abundant interactions are hydrophobic dispersive interactions. Dominant interaction in best pose of molecule **16d** is certainly hydrogen bonding with Gln725 (Fig. 7B). This interaction is probably the reason why the docking score of **16d** is slightly better than that of **16k** (−8.676 *vs.* −7.848). Actually, better docking score of **16d** is in line with our findings that **16d** more strongly interact with P-gp than **16k** (Fig. 5).

In addition, there are π–π stacking interactions with Trp232 and Phe343, as well as several π–alkyl hydrophobic interactions, with Phe336, Phe728 and Phe983 (Fig. 7B). Best docking pose for **16k** shows us mainly hydrophobic interactions, π–sigma with Phe343, π–sulphur with Met949, π–alkyl with Phe336, Phe983, and Met986 (Fig. 7D). We can see also π–anion interactions with Glu875 as well as hydrophobic interactions with Met986, Leu339, and Ala871.

Conclusions

Anticancer effects of pyrimidine derivatives and corresponding artesunate hybrid compounds studied in sensitive and MDR NSCLC cells demonstrated that hybrid compounds were more potent agents than the parent compounds artesunate and pyrimidines. Hybrid compounds **16a–k** were efficient in inducing cell growth inhibition of NCI-H460 cells with concentrations below 5 μM and they were all selective toward NCI-H460 cells. Especially, hybrids with piperazine linker **16h–k** were capable to evade MDR phenotype and inhibit P-gp activity. Among these four hybrid compounds, **16k** was the most potent with an IC_{50} value of 1.5 μM in NCI-H460 cells and a neglectable "Relative Resistance" factor of 1.1. Combined studies with DOX, a P-gp substrate, confirmed the inhibition of P-gp function by **16h–k**.

Experimental

General

Unless stated otherwise, all solvents and reagents were obtained from commercial sources and used without further purification. Dry-flash chromatography was performed on SiO_2 (0.018–0.032 mm). Melting points were determined on a Boetius PMHK apparatus and are not corrected. IR spectra were recorded on a Thermo-Scientific Nicolet 6700 FT-IR Diamond Crystal instrument. ^{1}H and ^{13}C NMR spectra were recorded on a Bruker Ultrashield Avance III spectrometer (at 500 and 125 MHz, respectively) and Varian 400/54 Premium Shielded spectrometer (at 400 MHz and 100 MHz, respectively). Chemical shifts were expressed in parts per million (ppm) on the (δ) scale. Chemical shifts were calibrated relative to those of the solvent. Optical rotations were measured on a Rudolph Research Analytical Autopol IV automatic polarimeter with dichloromethane as solvent, and the compound concentration used was 1.00 mg mL^{-1}. HRESIMS and MS/MS spectra were acquired in positive mode on Q Exactive Plus (ThermoFisher Scientific, Inc., Bremen, Germany) mass spectrometer, equipped with a heated HESI-II source. The synthesized compounds were also analyzed by high resolution tandem mass spectrometry using LTQ Orbitrap XL (Thermo Fisher Scientific Inc., USA) mass spectrometer. Compounds were analyzed for purity using Agilent 1200 HPLC system equipped with a Quat Pump

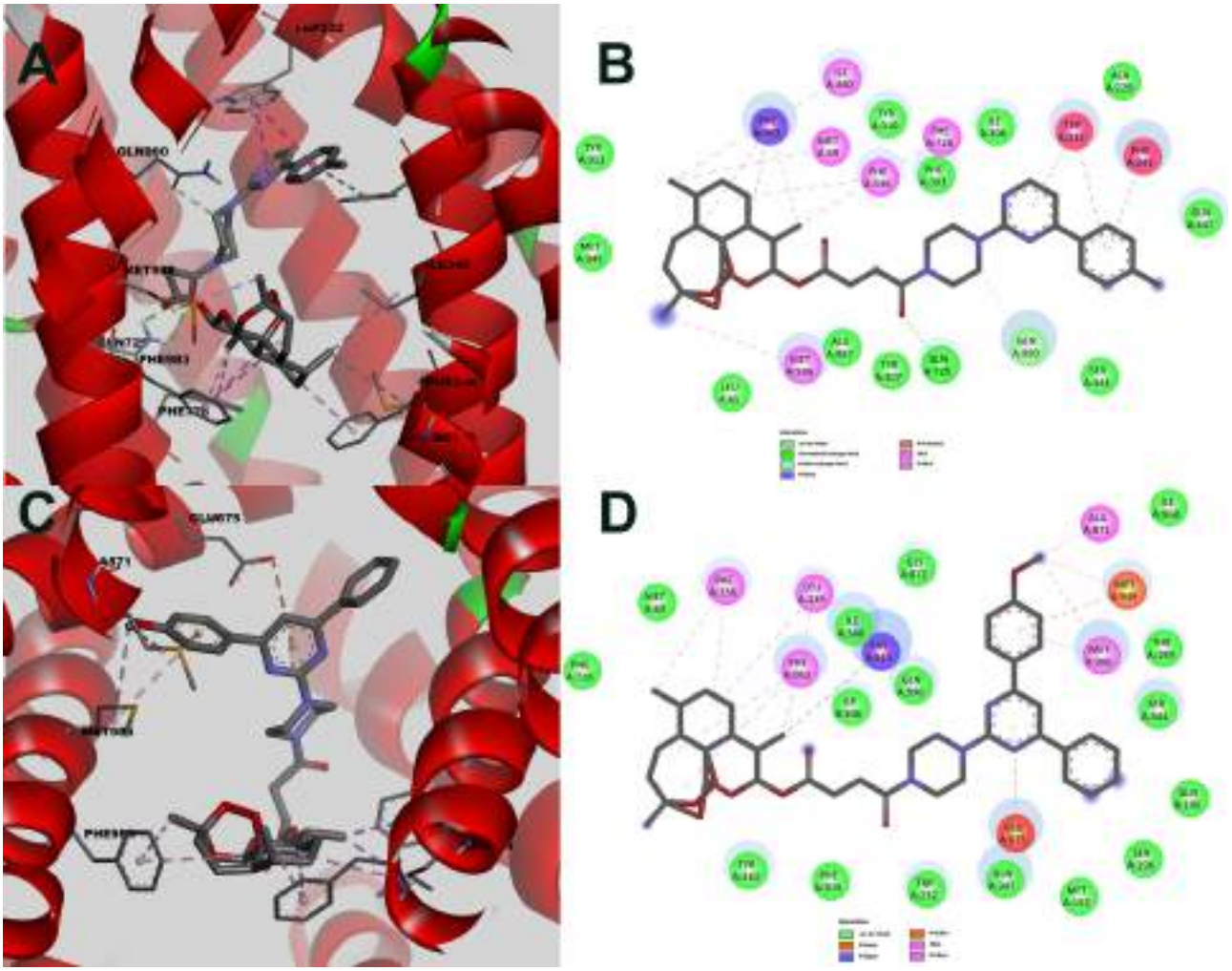

Fig. 7 Binding site of P-glycoprotein showing amino acid interactions with **16d** (A) and **16k** (C), and 2D scheme of ligand interactions of **16d** (B) and **16k** (D) with amino acids.

(G1311B), an injector (G1329B) 1260 ALS, TCC 1260 (G1316A) and a detector 1260 DAD VL+ (G1315C). All tested compounds are fully characterized and the purities were >95% as determined by HPLC (ESI†). HPLC purity analyses were performed in two diverse systems for each compound.

Chemistry

General procedure A for the Suzuki coupling reaction. The desired compounds **11a–i** were prepared according to the literature procedure.[25]

To a dry glass flask purged with argon $Pd(OAc)_2$ (0.05 eq.), PPh_3 (0.10 eq.) and appropriate solvent were added. The solution was stirred at room temperature for 5 min and appropriate 2,4-dichloropyrimidine **9** (1 eq.) and Na_2CO_3 (3.1 eq.) in H_2O (1.5 mL per 1.01 mmol of **9**) were added. After 5 min arylboronic acid **10** (1 eq.) was added and the reaction mixture was heated in an oil bath at 95 °C under inert atmosphere for 6 h. The solution was cooled to room temperature, washed with CH_2Cl_2 and dried over anhydrous Na_2SO_4. The organic solvent was removed under reduced pressure and the remaining solid was purified by dry-flash column chromatography.

General procedure B for nucleophilic aromatic substitution. The mono Boc-protected amines **12a–b** were synthesized according to the previously reported procedures.[26]

A mixture of **11** (1 eq.), appropriate monoprotected amine **12** (3 eq.) and K_2CO_3 (1.2 eq.) in dry 1,4-dioxane (2.8 mL per 0.37 mmol of **11**) was refluxed in an oil bath for 16 h under argon. The solution was cooled to room temperature, the residue was filtered and the solvent was removed under reduced pressure. The crude product was purified by dry-flash column chromatography and used in the next phase.

General procedure C for the deprotection of amino group. The deprotection of Boc-protected amine derivatives (1 eq.) was performed using trifluoroacetic acid (16 eq.) in CH_2Cl_2 (6.2 mL per 0.29 mmol of appropriate Boc-protected amine). The reaction mixture was stirred at room temperature for 15 h. After that, reaction mixture was neutralized with $NaHCO_3$ to pH 9 and extracted with CH_2Cl_2 (3 × 20 mL). The combined organic phases were washed with water and brine, dried over

anhydrous Na_2SO_4. The organic solvent was removed under reduced pressure to give the desired product which was directly used in the next step without further purification.

General procedure D for the synthesis of artesunate–pyrimidine hybrids. The dihydroartemisinin and artesunate were synthesized according to the reported procedures with slight modifications.[10] Hybrids were prepared according to the literature procedure.[27]

Artemisinin **1** (50 mg, 0.18 mmol) was dissolved in methanol (0.55 mL) and $NaBH_4$ (20 mg, 0.54 mmol) was added in portion at 0–5 °C over a period of 10 min. After being stirred for 90 min under the same reaction conditions, the mixture was neutralized to pH 6–7 using acetic acid and extracted with CH_2Cl_2 (3 × 15 mL). The combined organic phases were washed with water and brine, and dried over anhydrous Na_2SO_4. The organic solvent was removed under reduced pressure to give the desired product **2** (49 mg, 98%) as a colorless solid.

To a stirred solution of dihydroartemisinin **2** (1 eq.) in CH_2Cl_2 (3.7 mL) succinic anhydride (1.6 eq.) and imidazole (1.2 eq.) were added. After being stirred for 3 h on room temperature, 1 M HCl was added until pH 3 was reached. The reaction mixture was diluted with H_2O and extracted with CH_2Cl_2 (3 × 20 mL). The organic solution was washed with brine and dried over anhydrous Na_2SO_4. The organic solvent was removed under reduced pressure to give the desired product **5** which was directly used in the next step without further purification. Compound **5** was dissolved in CH_2Cl_2 (2.5 mL) and EDCI × HCl (1 eq.) and HOBt × H_2O (1 eq.) were added. The reaction mixture was stirred at room temperature for 1 h, after which the appropriate pyrimidine based amine **13a–f** or **14a–k** (1 eq.) was added and the resulting mixture was stirred at room temperature for 13 h. The solution was diluted with H_2O and the mixture was extracted with CH_2Cl_2 (3 × 15 mL) and dried over anhydrous Na_2SO_4. The organic solvent was removed under reduced pressure and the remaining solid was purified by dry-flash column chromatography.

Biological evaluation

Chemicals. RPMI 1640 medium, Minimum Essential Medium (MEM), and penicillin–streptomycin solution were purchased from Capricorn Scientific GmbH (Ebsdorfergrund, Germany), while the non-essential amino acids were purchased from Biowest (Nuaillé, France). Rhodamine 123 (Rho123), DMSO, thiazolyl blue tetrazolium bromide (MTT) and L-glutamine were obtained from Sigma-Aldrich Corporation (St. Louis, MO, USA). Trypsin/EDTA was purchased from Thermo Fisher Scientific (Grand Island, NY, United States).

Drugs. Tariquidar (TQ) was diluted in dimethyl sulfoxide (DMSO) while doxorubicin (DOX) was diluted in deionized water. Their 10 μM and 10 mM aliquots, respectively, were kept at −20 °C. Artemisinin, artesunate, pyrimidine derivatives and hybrid molecules were also diluted in DMSO and kept as 20 mM stocks at −20 °C. Working solutions for all compounds were prepared in sterile deionized water before the treatment.

Cells and cell culture. NCI-H460 (human non-small cell lung carcinoma) cell line was purchased from the American Type Culture Collection (ATCC, Rockville, MD). NCI-H460/R cells were selected from NCI-H460 cells by their continuous culturing in a medium with gradually increasing concentrations of doxorubicin.[28] Human lung fibroblasts (MRC-5) were purchased from the European Collection of Authenticated Cell Cultures (ECACC, Port Down, UK). NCI-H460 and NCI-H460/R cell lines were cultivated in RPMI 1640 medium supplemented with 10% fetal bovine serum, 2 mM L-glutamine, and 10 000 U mL^{-1} penicillin, 10 mg mL^{-1} streptomycin. MRC-5 cell line was cultivated in MEM supplemented with 10% fetal bovine serum, 2 mM L-glutamine, 2 mM non-essential amino acids and 5000 U mL^{-1} penicillin, 5 mg mL^{-1} streptomycin solution. All cells have been grown at 37 °C in a humidified 5% CO_2 atmosphere and sub-cultured after reaching the 80% confluence using 0.25% trypsin/EDTA.

MTT assay. Cell viability was assessed by (3-(4,5-dimethylthiazol-2-yl)-2,5-diphenyltetrazolium bromide) colorimetric assay (MTT assay) based on the reduction of tetrazolium dye into insoluble purple formazan in active mitochondria of living cells. Cells were seeded in 96-well tissue culture plates (2000 cells per well for NCI-H460, NCI-H460/R, and MRC-5) and incubated overnight in 100 μL of the compatible medium. Initially, cells were treated with 5 μM and 30 μM of artemisinin, artesunate, pyrimidine derivatives and hybrid molecules incubated for 72 h (37 °C, 5% CO_2). In the following experiments, to determine IC_{50} values, cells were treated with increasing concentrations of artemisinin, artesunate, pyrimidine derivatives and hybrid molecules (1, 2.5, 5, 10, 25 μM), and incubated for 72 h. The cell growth inhibitory effect of DOX increasing concentrations (100, 250, 500, 1000, and 2000) was also assessed in all employed cell lines. In addition, a single concentration of 50 nM TQ was simultaneously combined with **16a–g** (1, 2.5, 5, 10, 25 μM) while a single concentration of 500 nM **16h–k** was simultaneously combined with DOX (100, 250, 500, 1000, and 2000 nM) in NCI-H460/R cells, and also incubated for 72 h. After the treatment period, MTT was added in a final concentration of 0.2 mg mL^{-1} and incubated for 3 h at 37 °C, 5% CO_2. The resulting formazan dye was dissolved in (DMSO), 100 μL for NCI-H460, NCI-H460/R, and 50 μL for MRC-5. Using an automated microplate reader (Multiskan Sky, Thermo Scientific, Waltham, MA, USA), the absorbance of obtained dye was measured at 540 nm and 690 nm. The half-maximal inhibitory concentration (IC_{50}) of each compound was calculated using GraphPad Prism 8 (GraphPad Software. Inc., United States).

Rhodamine 123 accumulation assay. Accumulation of rhodamine 123, a fluorescent P-gp substrate, was analyzed by flow cytometry. Rhodamine 123 emits fluorescence whose intensity is proportional to the accumulated rhodamine 123. The assay was performed with artemisinin, artesunate, pyrimidine derivatives, hybrid molecules, and a P-gp inhibitor TQ in NCI-H460/R cells with high P-gp expression. NCI-H460 cells were used as a positive control for rhodamine 123 accumulation. NCI-H460/R cells were treated with tested compounds (5 μM), and TQ (50 nM) and incubated with rhodamine 123 (2 μM) for 30 min at 37 °C, 5% CO_2. For a concentration-dependent study,

NCI-H460/R cells were treated with increasing concentrations of artesunate, **16d**, and **16k** (2, 5, 10, and 20 μM) and tariquidar (2, 5, 10, and 20 nM). After the incubation period, cells were centrifuged and the remaining pellet was washed in PBS and placed in cold PBS. Rhodamine 123 accumulation was analyzed by CytoFLEX (Beckman Coulter, Inc., Brea, CA, USA). At least 10 000 events were assayed per sample.

***In silico* studies.** Wlog and TPSA values were generated using SwissADME web site.[33,34]

Protein structure PDB ID 6QEX was downloaded from RSCB database,[35,36] and prepared for docking using Schrödinger Suite 2021-1 Protein Preparation Wizard.[37] Small molecules were prepared using Maestro from Schrödinger Suite 2021-1.[38] Binding site was determined using previously published results[36] and docking simulations were performed using Glide from Schrödinger Suite 2021-1 using extra precision mode (XP).[39] Visualization and pictures were produced using Discovery Studio 2021 Client.[40]

Author contributions

Conceptualization was performed by IMO. LjK synthesized the compounds. NTJ, MN, PN and AT carried out NMR, HPLC and HRMS experiments. Biological part of the research was carried out by EL, MJ and MP. Docking simulations were performed by MZ. Supervision was performed by MN, MP and IMO. All authors contributed to the writing (review & editing).

Conflicts of interest

There are no conflicts to declare.

Acknowledgements

Financial support from the Ministry of Education, Science and Technological Development of the Republic of Serbia Contract numbers: 451-03-68/2022-14/200168, 451-03-68/2022-14/200026, 451-03-68/2022-14/200007 and Serbian Academy of Sciences and Arts grant F80. The authors are also thankful to the bilateral project of the Bulgarian Academy of Sciences (BAS) and the Serbian Academy of Sciences and Arts (SANU) named ''Phytochemical investigation of the secondary metabolites from plants and mushrooms and their biotransformation products''. The authors acknowledge the support of the FP7 RegPot project FCUB ERA GA no. 256716. The EC does not share responsibility for the content of the article.

Notes and references

1 D. J. Newman, *J. Med. Chem.*, 2008, **51**, 2589–2599.
2 T. Fröhlich, C. Mai, R. P. Bogautdinov, S. N. Morozkina, A. G. Shavva, O. Friedrich, D. F. Gilbert and S. B. Tsogoeva, *ChemMedChem*, 2020, **15**, 1473–1479.
3 S. Majhi and D. Das, *Tetrahedron*, 2021, **78**, 131801.
4 Z. Guo, *Acta Pharm. Sin. B*, 2017, **7**, 119–136.
5 C. Borsari, D. J. Trader, A. Tait and M. P. Costi, *J. Med. Chem.*, 2020, **63**, 1908–1928.
6 T. Fröhlich, A. Ç. Karagöz, C. Reiter and S. B. Tsogoeva, *J. Med. Chem.*, 2016, **59**, 7360–7388.
7 Y. Tu, *Angew. Chem., Int. Ed.*, 2016, **55**, 10210–10226.
8 (*a*) P. Buragohain, B. Saikia, N. Surineni, N. C. Barua, A. K. Saxena and N. Suri, *Bioorg. Med. Chem. Lett.*, 2014, **24**, 237–239; (*b*) O. P. S. Patel, R. M. Beteck and L. J. Legoabe, *Eur. J. Med. Chem.*, 2021, **213**, 113193.
9 J. Li and B. Zhou, *Molecules*, 2010, **15**, 1378–1397.
10 (*a*) L. Goswami, S. Paul, T. K. Kotammagari and A. K. Bhattacharya, *New J. Chem.*, 2019, **43**, 4017–4021; (*b*) Y. Zhou, X. Li, K. Chen, Q. Ba, X. Zhang, J. Li, J. Wang, H. Wang and H. Liu, *Eur. J. Med. Chem.*, 2021, **211**, 113000.
11 N. Ruwizhi, R. B. Maseko and B. A. Aderibigbe, *Pharmaceutics*, 2022, **14**, 504.
12 L. Botta, S. Filippi, C. Zippilli, S. Cesarini, B. M. Bizzarri, A. Cirigliano, T. Rinaldi, A. Paiardini, D. Fiorucci, R. Saladino, R. Negri and P. Benedetti, *ACS Med. Chem. Lett.*, 2020, **11**, 1035–1040.
13 S. Slezakova and J. Ruda-Kucerova, *Anticancer Res.*, 2017, **37**, 5995–6003.
14 M. Colombo, M. Giglio and I. Peretto, *J. Heterocycl. Chem.*, 2008, **45**, 1077–1081.
15 A. Dolšak, K. Mrgole and M. Sova, *Catalysts*, 2021, **11**, 439.
16 E. Venturini Filho, E. M. C. Pinheiro, S. Pinheiro and S. J. Greco, *Tetrahedron*, 2021, **92**, 132256.
17 WHO report on cancer: setting priorities, investing wisely and providing care for all, World Health Organization, Geneva, 2020, Licence: CC BY-NC-SA 3.0 IGO.
18 C. Allemani, T. Matsuda, V. Di Carlo, R. Harewood, M. Matz, M. Nikšić, A. Bonaventure, M. Valkov, C. J. Johnson, J. Estève, O. J. Ogunbiyi, G. Azevedo, E. Silva, W. Q. Chen, S. Eser, G. Engholm, C. A. Stiller, A. Monnereau, R. R. Woods, O. Visser, G. H. Lim, J. Aitken, H. K. Weir, M. P. Coleman and CONCORD Working Group, *Lancet*, 2018, **391**, 1023–1075.
19 Y. G. Assaraf, A. Brozovic, A. C. Gonçalves, D. Jurkovicova, A. Linē, M. Machuqueiro, S. Saponara, A. B. Sarmento-Ribeiro, C. P. R. Xavier and M. H. Vasconcelos, *Drug Resist. Updates*, 2019, **46**, 100645.
20 P. D. M. Juan-Carlos, P. P. Perla-Lidia, M. M. Stephanie-Talia, A. M. Mónica-Griselda and T. E. Luz-María, *Mol. Biol. Rep.*, 2021, **48**, 1883–1901.
21 C. Karthika, R. Sureshkumar, M. Zehravi, R. Akter, F. Ali, S. Ramproshad, B. Mondal, P. Tagde, Z. Ahmed, F. S. Khan, M. H. Rahman and S. Cavalu, *Life*, 2022, **12**, 897.
22 D. P. Kodack, A. F. Farago, A. Dastur, M. A. Held, L. Dardaei, L. Friboulet, F. Flotow, L. J. Damon, D. Lee, M. Parks, R. Dicecca, M. Greenberg, K. E. Kattermann, A. K. Riley, F. J. Fintelmann, C. Rizzo, Z. Piotrowska, A. T. Shaw, J. F. Gainor, L. V. Sequist, M. J. Niederst, J. A. Engelman and C. H. Benes, *Cell Rep.*, 2017, **21**, 3298–3309.
23 L. Chen, C. Wang, N. Hu and H. Zhao, *RSC Adv.*, 2019, **9**, 1004–1014.
24 L. Gruber, S. Abdelfatah, T. Fröhlich, C. Reiter, V. Klein, S. B. Tsogoeva and T. Efferth, *Molecules*, 2018, **23**, 841.

25 T. Taldone, Y. Kang, H. J. Patel, M. R. Patel, P. D. Patel, A. Rodina, Y. Patel, A. Gozman, R. Maharaj, C. C. Clement, A. Lu, J. C. Young and G. Chiosis, *J. Med. Chem.*, 2014, **57**, 1208–1224.

26 (*a*) I. A. Moussa, S. D. Banister, C. Beinat, N. Giboureau, A. J. Reynolds and M. Kassiou, *J. Med. Chem.*, 2010, **53**, 6228–6239; (*b*) X. Elduque, E. Pedroso and A. Grandas, *J. Org. Chem.*, 2014, **79**, 2843–2853.

27 N. Wang, K. J. Wicht, E. Shaban, T. A. Ngoc, M. Q. Wang, I. Hayashi, I. Hossain, Y. Takemasa, M. Kaiser, I. T. Sayed, T. J. Egan and T. Inokuchi, *Med. Chem. Commun.*, 2014, **5**, 927–931.

28 M. Pesic, J. Z. Markovic, D. Jankovic, S. Kanazir, I. D. Markovic, L. Rakic and S. Ruzdijic, *J. Chemother.*, 2006, **18**, 66–73.

29 D. Duarte, M. Nunes, S. Ricardo and N. Vale, *Biomolecules*, 2022, **12**, 1490.

30 A. Podolski-Renić, M. Jadranin, T. Stanković, J. Banković, S. Stojković, M. Chiourea, I. Aljančić, V. Vajs, V. Tešević, S. Ruždijić, S. Gagos, N. Tanić and M. Pešić, *Cancer Chemother. Pharmacol.*, 2013, **72**, 683–697.

31 C. Reiter, T. Fröhlich, L. Gruber, C. Hutterer, M. Marschall, C. Voigtländer, O. Friedrich, B. Kappes, T. Efferth and S. B. Tsogoeva, *Bioorg. Med. Chem.*, 2015, **23**, 5452–5458.

32 (*a*) A. Daina and V. Zoete, *ChemMedChem*, 2016, **11**, 1117–1121; (*b*) A. Daina, O. Michielin and V. Zoete, *Sci. Rep.*, 2017, **7**, 42717.

33 **https://www.swissadme.ch/**.

34 A. Daina, O. Michielin and V. Zoete, *Sci. Rep.*, 2017, **7**, 42717.

35 **https://www.rcsb.org/structure/6QEX**.

36 A. Alam, J. Kowal, E. Broude, I. Roninson and K. P. Locher, *Science*, 2019, **363**, 753.

37 Schrödinger Release 2021-1: Protein Preparation Wizard; Epik, Schrödinger, LLC, New York, NY, 2021; Impact, Schrödinger, LLC, New York, NY; Prime, Schrödinger, LLC, New York, NY, 2021.

38 Schrödinger Release 2021-1: Maestro, Schrödinger, LLC, New York, NY, 2021.

39 Schrödinger Release 2021-1: Glide, Schrödinger, LLC, New York, NY, 2021.

40 BIOVIA, Dassault Systèmes, Discovery Studio 2021 Client, Dassault Systèmes, San Diego, 2021.